LES OF SWIRLING FLOW IN SEPARATION DEVICES

Jos Derksen
Kramers Laboratorium voor Fysische Technologie
Delft University of Technology
Prins Bernhardlaan 6, 2628 BW Delft, The Netherlands
jos@klft.tn.tudelft.nl

ABSTRACT

Large-eddy simulations (LES) of confined swirling flow with applications in cyclone separators are presented. First, the quality of the LES is assessed by means of experimental data obtained by Escudier et al. (1980) of the flow in a swirl-tube-geometry. Results with three subgrid-scale models, and three spatial resolutions will be compared. Consecutively, the turbulent flow in a cyclone separator used in industrial practice (a Stairmand high-efficiency cyclone) has been simulated. Good agreement in terms of the time-averaged flow, and in terms of the flow's dynamic behavior was obtained. Finally, the applicability of the LES flow field for performing particle separation calculations is demonstrated.

INTRODUCTION

Swirling flows are applied in many industrial processes. Examples can be found in combustion, turbomachinery, mixing, and separation. The work presented here has its motivation in cyclone separators for cleaning gas streams contaminated with solid particles (Hoekstra et al., 1999; Derksen and Van den Akker, 2000). The driving force for separation is the centrifugal force induced by a confined, strongly swirling gas flow. The performance of the separator therefore fully relies on the flow field. The scale of the equipment applied in industrial practice is such that turbulence is a key issue. Flow simulation is one of the tools that are employed in the quest towards separation efficiency improvement and/or energy consumption (i.e. pressure drop) reduction. Reliable prediction of the equipment's separation performance is not an easy task, since it requires an accurate simulation of a turbulent, two-phase flow in a complex geometry. If one operates the cyclone under low solids loading conditions, one-way coupling between the continuous gas phase and the dispersed solid phase can be assumed, which reduces the modeling task to the single-phase turbulent gas flow field, and the impact it has on solid particle motion.

For two reasons, a large-eddy approach to turbulence modeling was pursued. In the first place, vortex flows are often associated with coherent oscillations (the "vortex whistle", or vortex core precession) that have frequencies that interfere with the low-frequency part of the turbulence spectrum. In the second place (with a view to gas-solid applications), calculating solid particle transport does not need much additional modeling if one is able to resolve the flow down to the relaxation time (and associated length scales) of the particles.

In the first part of the paper, some numerical and subgrid-scale modeling issues will be addressed in relation to an experimentally extensively studied confined swirling flow, i.e. the swirl tube geometry due to Escudier et al. (1980). In the second part of the paper, an LES of the flow inside an industrial cyclone geometry, i.e. a Starimand high-efficiency cyclone (Stairmand, 1951) operating at a typical pilot-plant-scale Reynolds number (Re=280,000) is presented, along with a study of solid particle motion based on one-way coupling with the gas flow.

MODELING ISSUES

The simulations make use of lattice-Boltzmann discretization of the Navier-Stokes equations. Lattice-Boltzmann methods are relatively cheap methods to simulate fluid flow in geometrically complex configurations (Chen and Doolen, 1998). The scheme we use represents the incompressible Navier-Stokes equations with second-order accuracy (in space and time). The method that we have applied is based on a uniform, cubic lattice. The computer code runs very efficiently on moderately sized (20 cpu's) Beowulf clusters.

The swirl tube flow has been simulated with three different subgrid-scale models, *viz.* the standard Smagorinsky model with c_S=0.1 (Smagorinsky, 1963), a model due to Voke (1996), and a mixed-scale model as discussed by Sagaut et al. (2000). The Stairmand cyclone simulations were performed exclusively with the Smagorinsky model (c_S=0.1).

The Voke model is specifically designed for flows with regions that have low mesh Reynolds numbers r ($r=\frac{\Delta^2\left(2\bar{s}_{ij}\bar{s}_{ij}\right)^{1/2}}{\nu}$, with Δ the grid-spacing, ν the kinematic viscosity, and $\bar{s}_{ij}$ the resolved rate of strain tensor), where it reduces the eddy viscosity compared to the standard Smagorinsky model. A key feature of confined swirling flow is the vortex core that nearly behaves as a solid body rotation, with hardly any deformation. It is therefore anticipated that a model that is more selective than the Smagorinsky model may improve the results.

The eddy viscosity in the mixed-scale model (ν^e_{MSM}) is a mixture of the Smagorinsky eddy viscosity (ν^e_{Sm}), and the eddy viscosity from the turbulent kinetic energy model (ν^e_{TKE}):

$$\nu^e_{MSM}=\sqrt{\nu^e_{Sm}\nu^e_{TKE}} \qquad (1)$$

with $\nu^e_{TKE}=c\Delta\sqrt{\frac{1}{2}\left[\left(\tilde{\bar{u}}_i-\bar{u}_i\right)\left(\tilde{\bar{u}}_i-\bar{u}_i\right)\right]}$ (Sagaut et al., 2000). The term under the square-root sign is the kinetic energy of the test field with $\bar{u}_i$ the resolved velocity, and $\tilde{\bar{u}}_i$ the velocity field after applying a low-pass test filter with width 2Δ. The constant c amounts to 0.01.

All simulations discussed here applied Van Driest wall damping functions (Hinze, 1959) to explicitly bring the eddy-viscosity to zero in the vicinity of no-slip walls.

SWIRL TUBE SIMULATIONS

Flow System

The flow geometry (Escudier, 1980) is given in Figure 1. In this figure, a coordinate system, and the nomenclature with respect to the geometrical dimensions (D, D_e, L, L_e, t, and L_i) are defined. The definition of the Reynolds number is based on the conditions at the inlet: $Re=U_{in}t/\nu$, with U_{in} the (superficial) inlet velocity ($U_{in}=Q/Lt$, with Q the volumetric flow rate). The Reynolds number in the simulations, as well as most of the experiments amounted to 1,900. The Reynolds number in e.g. the exit tube is much higher: with the information as given in Figure 1 one can derive that $Re_e\equiv\frac{4Q}{\pi D_e\nu}=14.6Re$.

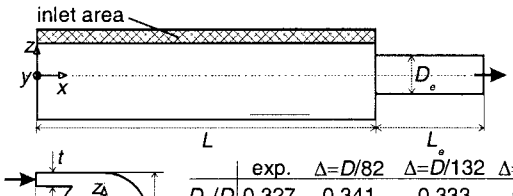

	exp.	Δ=D/82	Δ=D/132	Δ=D/184
D_e/D	0.327	0.341	0.333	0.326
L/D	3.791	3.787	3.792	3.791
t/D	0.145	0.146	0.151	0.141
L_e/D	1.509*	1.457	1.390	1.427
L_i/D	n.a.	0.250	0.223	0.236

*open outflow

Figure 1. Swirl tube geometry defined by Escudier et al. (1980). Fluid enters through a tangential slit with superficial velocity U_{in}, and exits through a

In a previous paper (Derksen, 2002), it has been demonstrated that by using the Smagorinsky model we could reproduce the strong impact on the entire flow of a reduction of the exit pipe diameter D_e in accordance with experimental data. In the present paper, the focus will be on comparing different subgrid-scale models, and spatial resolutions, at a single exit pipe diameter (D_e/D=0.33).

The simulations were carried out at three different spatial resolutions: $\Delta=D/82$, $\Delta=D/132$, and $\Delta=D/184$. The lattices were uniform and cubic. In order to have an integer number of lattice spacings Δ in the vortex chamber diameter D, and in the exit pipe diameter D_e, the values for the D_e/D ratios slightly deviate from the experimental values (see the table in Figure 1). At the solid walls, no-slip boundary conditions were imposed. At the inlet area, the velocity in the y-direction was fixed to a parabolic function of the z-coordinate, and a uniform function of the x-coordinate; the x- and z-component of the velocity were set to zero. At the outlet, a zero-gradient boundary condition was imposed.

Results

Flow visualizations (Escudier et al., 1980) revealed the occurrence of a bubble type vortex breakdown (Type 0 in the classification by Faler and Leibovich, 1977) in the exit pipe in

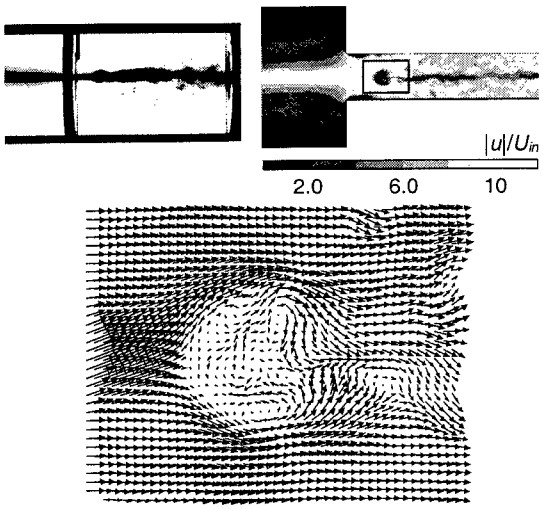

Figure 2. Vortex breakdown. Top-left: visualization as reported by Escudier et al. (1980) Re=1,600. Top-right: LES snapshot in terms of the contours of the absolute value of the velocity near the contraction at Re=1,900. Bottom: the velocity vector field at the position as indicated with the rectangles in the top right image.

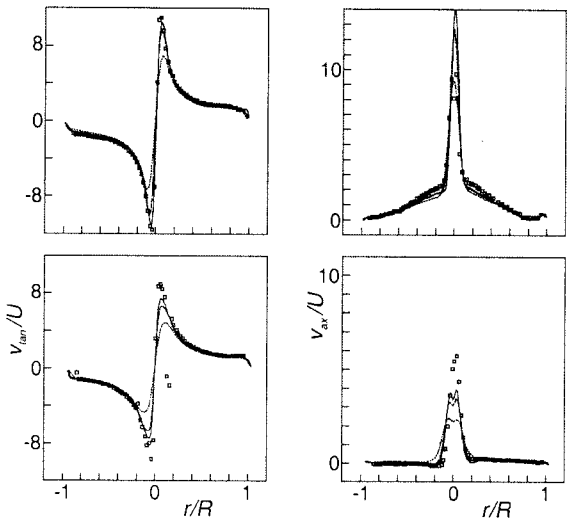

Figure 3. Average velocity profiles along the radius of the swirl tube. Left: tangential velocity; right: axial velocity. Comparison between experiments (symbols), LES with grid spacing $\Delta=D/184$ (solid lines), $\Delta=D/132$ (long dashed lines), and $\Delta=D/82$ (short dashed lines). Bottom graphs: $x=0.7D$; top graphs: $x=3.6D$.

the $D_e/D=0.33$ geometry at $Re=1{,}600$. The LES resolves this flow feature very well, see Figure 2. It clearly shows the Type 0 breakdown, with a single, thin tail. The bubble is filled and emptied simultaneously at the rear part (see the vector plot in Figure 2). Also the transition from laminar-like flow upstream of the vortex breakdown, to turbulent flow downstream is well represented by the LES.

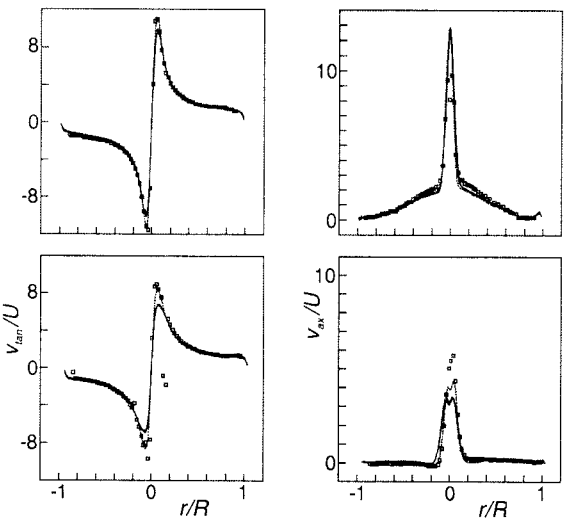

Figure 4. Average velocity profiles along the radius of the swirl tube with $\Delta=D/132$. Left: tangential velocity; right: axial velocity. Comparison between experiments (symbols), and three subgrid-scale models: Smagorinsky model (solid line); Voke model (long-dash); mixed-scale model (short dash). Bottom graphs: $x=0.7D$; top graphs: $x=3.6D$.

The average velocity profiles in Figure 3 and 4 show high gradients. Increasing the spatial resolution helps in a better representation of the profiles (Figure 3). When mutually comparing the three subgrid-scale models (Figure 4), the model due to Voke (1996) does not have significant advantage over the standard Smagorinsky model. The mixed-scale model does show improvement. The maximum tangential velocity gets predicted accurately (even better than the predictions by the Smagorinsky model on the finest grid), whereas the extent to which the axial velocity at the $x=0.7D$ position is underestimated reduces appreciably.

STAIRMAND HIGH-EFFICIENCY CYCLONE

Flow system

The classical Stairmand high-efficiency cyclone geometry (Stairmand, 1951) has been depicted in Figure 5. As in the swirl tube, the main vortex is created by letting the flow into the equipment through a tangential inlet channel. The conical shape of the vortex chamber is meant to maintain high tangential velocities throughout the chamber. The bin underneath the conical section is the dust collector. The exit pipe (a.k.a. vortex finder) is placed at the top, which makes this cyclone of the reverse-flow type: the flow in the axial direction reverses.

The flow conditions of the LES have been chosen such that they conform with the experiments performed by Hoekstra (2000). He performed LDA measurements of the tangential and axial velocity at various locations in the cyclone at $Re=280{,}000$ (with $Re=U_{in}D/\nu$). The uniform, cubic lattice had a spacing of $\Delta=D/90$.

In contrast to the swirl tube simulations, the zero-gradient exit boundary condition gave rise to unphysical solutions, starting in the vicinity of the exit boundary, and gradually propagating upstream. The problems are most likely due to the subcriticality of the flow at the exit plane caused by the swirling motion (Escudier et al., 1982). By placing an obstacle in the exit pipe (see Figure 5), the subcritical flow turns to supercritical at the exit plane (as already suggested by Benjamin, 1962). It was checked to what extent the size and exact location of the obstacle did influence the overall flow field predictions. No significant effects were observed, unless the obstacle was too small and the subcritical flow extended to the outflow plane

Flow Field Results

A comparison between experimental (Hoekstra, 2000), and LES velocity profiles is presented in Figure 6. In terms of the average tangential and axial velocity, the agreement between experiment and simulation is good. The size of the vortex core (the region near the center with solid body rotation), as well as the maximum tangential velocity (important for particle separation) are resolved well. The subtle details in the experimental axial velocity profiles are represented fairly well in the LES. The agreement in terms of the RMS velocity

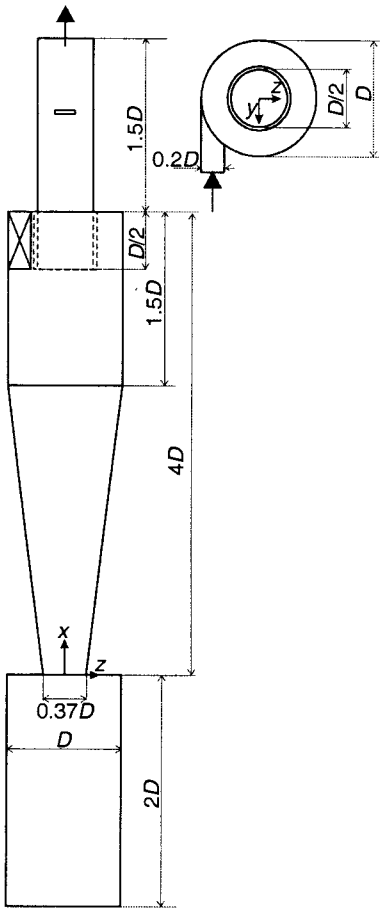

Figure 5. Stairmand cyclone geometry, dimensions and coordinate system. Left: side view; right: top view.

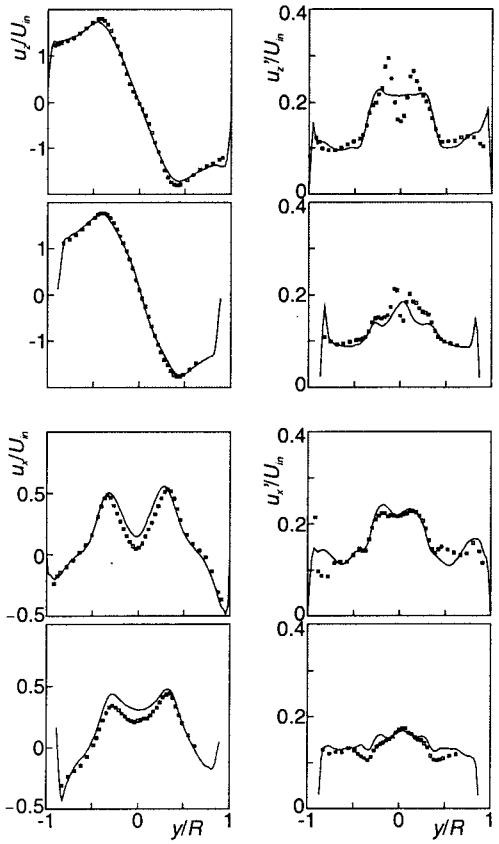

Figure 6. Radial velocity profiles in the Stairmand cyclone along the y-direction. Top-4 profiles: average tangential (left) and RMS tangential velocity (right) at x=3.25D (top), and x=2.0D (bottom). Bottom-4 profiles: same but now for the axial velocity. The symbols denote LDA experiments (Hoekstra, 2000), the lines are the LES results.

profiles is less good, albeit that apparently also the experiments show higher uncertainty here.

A striking phenomenon in the RMS profiles is their higher level close to the center. This is due to vortex core precession: a low-frequency, quasi-periodic, precessing motion of the vortex core. When measuring the velocity at a fixed position in space, it gives rise to periodic fluctuations. This is illustrated in Figure 7, in terms of power spectra of the velocity fluctuations. The experimental spectrum shows two clear peaks, at S=0.70 and S=1.58 (with S the Strouhal number defined as $S=fD/U_{in}$, with f the frequency). The LES is capable of resolving the latter peak (in the LES the peak frequency is S=1.61). So far, the reason for not resolving the former peak by the LES is unknown.

Solid Particle Separation

To numerically study the collection efficiency of the Stairmand high-efficiency cyclone, particles were released in the LES flow field. The particles were considered to be spherical entities that experience gravity (without buoyancy; the applications relate to gas-solid systems), and Stokes-drag. One-way coupling was assumed, and particle-particle collisions were discarded, albeit that mass loading effects on cyclone separation performance have been witnessed for mass loadings as low as 1% (Ontko, 1996), i.e. at very low particle

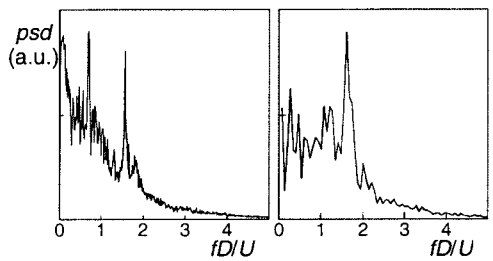

Figure 7. The power spectral density (*psd*) of the tangential velocity near the center of the Stairmand cyclone. Left: LDA experiment; right: LES.

volume fractions (of the order of 10^{-5}).

The above assumptions imply that (given the flow geometry) the gas-solid flow problem is fully defined by three dimensionless numbers: the gas-flow's overall Reynolds number (*Re* as defined above), the particle's Stokes number ($Stk = \frac{\rho_p}{\rho_g}\frac{d_p^2 U_{in}}{18\nu D}$, with d_p the particle diameter, and $\frac{\rho_p}{\rho_g}$ the particle over gas density ratio), and the Froude number ($Fr = \frac{U_{in}^2}{D|\mathbf{g}|}$, with $\mathbf{g}$ the gravitational acceleration vector).

At Re=280,000, and Fr=90 (these conditions relate to the experimental conditions of Hoekstra, 2000), 23 sets each consisting of 12,000 identical particles were tracked through the cyclone. The 23 Stokes numbers are in the range $Stk=5\cdot10^{-6}$ to 0.39. The particles were released at the inlet area, where they were uniformly distributed. Feeding particles was started at t=0 in a fully developed flow. At $t=18D/U_{in}$ adding new particles was stopped. Every time step, the particle positions were updated according to the following equation:

$$\frac{d\mathbf{v_p}}{dt} = \frac{U_{in}}{Stk\ D}\left(\mathbf{u} - \mathbf{v_p}\right) + \mathbf{g} \qquad (2)$$

with $\mathbf{v_p}$ the particle velocity vector, and $\mathbf{u}$ the gas velocity at the location of the particle. In general $\mathbf{u}$ is composed of a resolved and an unresolved part. The resolved part is linearly interpolated to the position of the particle; the unresolved part is estimated by a stochastic process with a variance related to the (estimated) subgrid-scale kinetic energy. Equation 2 was time-discretized according to an Euler-implicit scheme. Equally sized time steps were applied in the LES, and the particle update algorithm. All particle-wall collisions were considered to be fully elastic. Once a particles crossed the plane x=5.5D (i.e. the outflow boundary), it was considered to be exhausted.

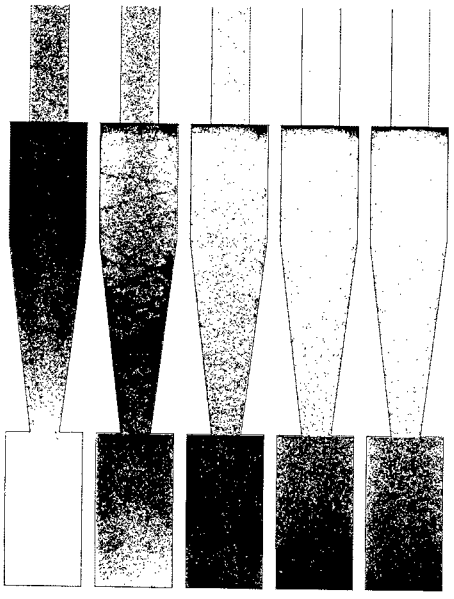

Figure 8. Side view of the cyclone with the particles at 5 moments in time. From left to right: tU_{in}/D=18, 51, 90, 152, and 228.

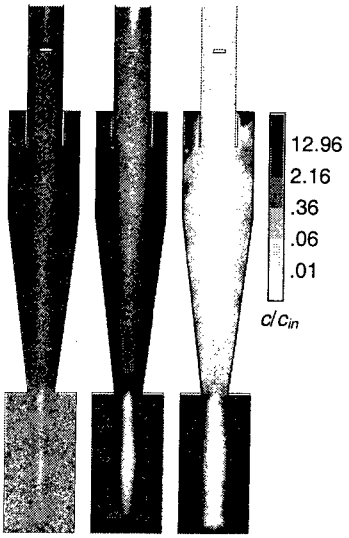

Figure 9. Time-averaged particle concentration in the x-z plane at y=0, at three Stokes numbers. From left to right $Stk=6.5\cdot10^{-5}$, $1.4\cdot10^{-3}$, and $3.0\cdot10^{-2}$.

Figure 8 shows the time evolution of the particle transport process. The moment $t=18D/U_{in}$ corresponds to the end of the time interval during which particles were fed into the cyclone. Spiral-shape structures can be observed at the outer wall of the cyclone body. This feature strongly resembles observations in our transparent experimental facility. At $t=228D/U_{in}$ still a considerable amount of particles has neither been exhausted, nor collected (if we define particle collection as a particle being inside the collection bin; particle collection defined this way is not definitive since it has been observed that in some occasions particles exit the collection bin). Most of the particles that are still inside the cyclone body are captured in a recirculation region in the annulus in between the exit pipe and the cyclone wall, near the top of the cyclone body.

A more quantitative view on cyclone operation is given in Figure 9: the smaller particles (i.e. with the lower Stokes numbers) get dispersed in the cyclone and are then likely to be caught by the (on average upward) flow in the core of the cyclone, and exit through the vortex finder. It is interesting to see how the (bigger) particles with $Stk=3.0\cdot10^{-2}$ behave in the inlet/exit-pipe region. In the inlet area, they are homogeneously dispersed as a result of the imposed inlet conditions. They do not attach immediately to the wall once they enter the body of the cyclone, as the still bigger particles do (not shown), but have some chance to enter the weak shortcut flow that directly guides gas from the annulus in between the vortex finder and the cyclone wall into the exit

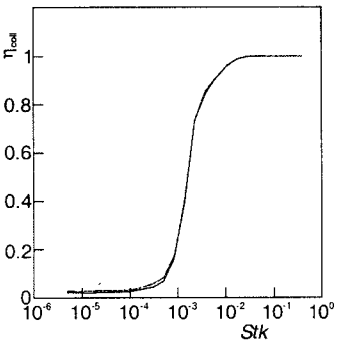

Figure 10. Simulated particle collection efficiency as a function of the particle Stokes number *Stk*. Solid line: particle motion not influenced by subgrid-scale gas velocity; dashed line: particles feel subgrid-scale gas velocity by means of a random process.

pipe and get exhausted. A recirculation due to boundary layer separation at the bottom of the inlet channel plays a prominent role in this process: its presence acts as an obstacle and enhances shortcut flow. As a result, at the side of the recirculation (the left-hand-side of the cyclones in Figure 9) relatively many particles with $Stk=3.0\cdot10^{-2}$ enter the exit pipe. Also quite some particles with $Stk=3.0\cdot10^{-2}$ get detached from the wall in the bottom part of the conical section due to the high turbulent activity in this part of the flow.

The collection efficiency (or grade-efficiency) curves (Figure 10) indicate a cut-size corresponding to $Stk_{50}=1.5\cdot10^{-3}$ (the cut size of a cyclone is defined as the particle size that for 50% gets collected). From Figure 10 it can be concluded that there is little difference between simulations with and without the particles feeling the subgrid-scale motion: Apparently the LES grid was sufficiently fine, and/or the particles sufficiently big for the subgrid-scale motion not to influence the separation process.

CONCLUSIONS

LES of strongly swirling flows have been performed, with a strong emphasis on experimental validation. Spatial resolution and subgrid-scale modeling issues were discussed in relation to a swirl tube geometry due to Escudier (1980). Most remarkable here was the improvement of the predictions when using a mixed-scale model.

The LES flow field determined in a Stairmand high-efficiency cyclone was used to predict the collection performance of this separation device. It was demonstrated that the subgrid-scale motion had little impact on the solid particle transport in the cyclone, illustrating the potential of LES for realistic descriptions of practical gas-solid flows.

REFERENCES

Benjamin, T.B., 1962, "Theory of the vortex breakdown phenomenon", *Journal of Fluid Mechanics*, Vol. 14, pp. 593-629.

Chen, S., and Doolen, G.D., 1998, "Lattice-Boltzmann method for fluid flows", *Annual Review Fluid Mechanics*, Vol. 30, pp. 329-364.

Derksen, J., and Van den Akker, H.E.A., 2000, "Simulation of vortex core precession in a reverse-flow cyclone", *AIChE Journal*, Vol. 46, pp. 1317-1331.

Derksen, J.J., 2002, "Large-eddy simulations on confined swirling flow" *Proceedings, 5th International Symposium on Engineering Turbulence Modelling and Measurement*, W. Rodi, ed., Elsevier, Amsterdam, pp. 907-916.

Escudier, M.P., Bornstein, J., and Zehnder, N., 1980, "Observations and LDA measurements of confined turbulent vortex flow", *Journal of Fluid Mechanics*, Vol. 98, pp. 49-63.

Escudier, M.P., Bornstein, J., and Maxworthy, T., 1982, "The dynamics of confined vortices". *Proceedings of the Royal Society London A*, Vol. 382, pp. 335-360.

Faler, J.H., and Leibovich, S., 1977, "Disrupted states of vortex flow and vortex breakdown", *Physics of Fluids*, Vol. 20, pp. 1385-1400.

Hinze, J.O., 1959, "Turbulence", McGraw-Hill, New York.

Hoekstra, A.J., Derksen, J.J., and Van den Akker, H.E.A., 1999, "An experimental and numerical study of turbulent swirling flow in gas cyclones", *Chemical Engineering Science*, Vol. 54, pp. 2055-2065.

Hoekstra, A.J., 2000, "Gas flow field and collection efficiency of cyclone separators", Ph.D. Thesis, Delft University of Technology, The Netherlands.

Ontko, J.S., 1996, "Cyclone separator scaling revisited", *Powder Technology*, Vol. 87, pp. 93-104.

Sagaut, P., Comte, P., and Ducros, F., 2000, "Filtered subgrid-scale models", *Physics of Fluids*, 12, pp. 233-236.

Smagorinsky, J., 1963, "General circulation experiments with the primitive equations: part I, the basic experiment", *Monthly Weather Review*, Vol. 91, pp. 99-164.

Stairmand, C.J., 1951, "The design and performance of cyclone separators", *Transactions IChemE*, Vol. 29, pp. 356-383.

Voke, P.R., 1996, "Subgrid-scale modelling at low mesh Reynolds number", *Theoretical and Computational Fluid Dynamics*, Vol. 8, pp. 131-143.